11^{th} International Conference on Fracture Mechanics of Concrete and Concrete Structures
FraMCoS-11
J. M. Chandra Kishen, A. Ramaswamy, S. Ray and R. Vidyasagar (Eds)
https://doi.org/10.21012/FC11.0923108

MODELING ANISOTROPIC FRACTURE IN QUASI-BRITTLE MATERIALS BY A PHASE FIELD APPROACH

Mrunmayee S.*, Amirtham Rajagopal† AND Pranavi D.‡

*Indian Institute of Technology
Hyderabad
e-mail: mrunmayee.shiradhonkar@gmail.com

†Indian Institute of Technology
Hyderabad
e-mail: rajagopal@ce.iith.ac.in

‡Indian Institute of Technology
Hyderabad
e-mail: pranavijaan1996@gmail.com

Key words: Phase field approach, Mixed-mode, Anisotropic fracture

Abstract. The main aim of the current study is to explore direction-dependent fracture initiation and propagation within an arbitrary anisotropic solid. In particular, the specific objective is to develop an anisotropic cohesive phase-field (PF) fracture model. The anisotropy in fracture due to mixed-mode conditions. A power law-inspired fracture criterion is adopted and it captures the dominating mode behavior of fracture. A volumetric-deviatoric energy split has been implemented to capture the impacts of mixed modes. The performance of the model is demonstrated through numerical examples to predict anisotropic fracture in quasi brittle materials such as rock and wood under mixed mode loading conditions. The numerical results are validated by comparing with experimental results available in litreature.

1 INTRODUCTION

Fracture in materials like composites, wood, and polycrystalline materials is anisotropic in nature. Anisotropy is the property of being directionally dependent. It is defined as the difference in the physical property of a certain material when measured along different axes. The directional dominance in the material due to anisotropy can be classified as structural, magnetic, or induced. Structural anisotropy may be attributed to the presence of fibers, grain boundaries, voids, defects in polycrystalline materials, and crystallographic orientation. Various types of composites, polycrystals, wood, and layered rocks like shales and sandstones are some examples of materials that are structurally anisotropic. Some examples of materials with induced anisotropy include the Strong anisotropic behavior of Ferromagnetic materials processed in a magnetic field [1]. Magnetic anisotropy can be seen for materials when magnetic properties vary in the different orientations [2]. The anisotropic fracture can be modeled by incorporating an orientation-dependent critical fracture energy function $G_c(\theta)$. Anisotropy can be broadly classified into (a) weak anisotropy (like in transversely isotropic materials or like in orthotropic materials having one or two independent fiber orientations) and (b) strong anisotropy (like in

materials with cubic symmetry, materials with sawtooth crack patterns, like those observed in thin anisotropic sheets [3]). The weak or strong anisotropic systems can be defined from the polar plot of inverse fracture toughness $1/G_c(\theta)$. For simulating fracture in weakly anisotropic materials, like fiber-reinforced composites having one or two fiber families, a convex fracture energy function, $G_c(\theta)$ is sufficient, whereas, to model the fracture in thin anisotropic sheets, where the crack path is unstable, and results in sawtooth type patterns and crack kinking, defining a non-convex fracture energy function, $G_c(\theta)$ is essential. Furthermore, the direction of the crack path is dependent on the state of stress near the crack tip. Crack propagation and path can vary based on the loading direction, stating the varying stress state and, in turn, anisotropy in the stress state. Apart from material directionality, an anisotropic fracture thus results from a variable stress state and energy release rate due to loading conditions. In summary, for a material, three levels of anisotropy can thus be seen: the presence of anisotropy, like the stress state, fracture toughness, and material orientation itself.

Phase field models have been adopted to model both weakly anisotropic [4, 5] and strongly anisotropic materials [6, 7]. In [7], the effective length scale parameter $l(\xi, \theta)$ have been defined in terms of crack orientation θ and fiber orientation ξ for three cases, namely, (a) transversely isotropic, (b) orthotropic, and (c) cubic anisotropy. The stress state-induced anisotropy at the crack tip is captured using a structural tensor to give the direction to the crack [8]. As the material's weak plane is the possible fracture direction, this tensor considers the crack angle in a weak plane. For materials like composite, which have the directionality present due to fiber orientation, the structural tensor is used to denote fiber direction in material [4, 9]. In the case of aluminum sheets, the directionality imparted due to the rolling of these sheets governs the fracture path [10]. Piezoelectric materials have high directionality in the poling direction. The tensor present in the crack surface density function considers the poling guidance, its perpendicular direction, and respective fracture toughness values. This term captures the anisotropic behavior of fracture toughness [11]. The favored fracture direction is the one along the minimum fracture energy value. The anisotropic fracture toughness incorporates crack projection in the most vulnerable plane, and a maximum energy release rate criterion is employed for crack direction prediction [12]. Direction-dependent fracture toughness at atomistically calibrated scales can be calculated based on crack direction and material directionality using a phase field approach [13]. Anisotropic fracture in crystallographic materials is captured by introducing an anisotropic term using damage gradients in fracture energy [14]. Phase field framework is used in a variety of fracture problems [15–17]. In a phase field approach, different decomposition and energy split methods are attempted in literature [18, 19]. Energy splits are used with different fracture criteria, such as the B-K [20] and power law criteria [21], which define the driving force for mixed-mode fracture. These models capture the mixed-mode effects and effectively show the fracture corresponding to the dominating state of stress [22–24].

In this present work, we present a phase field approach for modeling mixed-mode fracture in a weakly anisotropic material. This is achieved by considering a second-order structural tensor in the crack density function. A mixed-mode approach that uses a power-law for combining the modes is adopted from the litreature [24]. A volumetric-deviatoric split of energy is used to define the terms driving the fracture corresponding to modes I and II. The evolution of fracture is tracked by adopting a staggered scheme. The proposed model is applied to investigate a) anisotropic fracture in rock-like materials with multiple fissures under mixed-mode conditions and b) the role of mode mixity on the mixed-mode anisotropic fracture behavior of Russian pine wood. The paper is organized as follows in section 2 we discuss the methodology of the phase field formulation. In section 3

we present the numerical examples. In the last section the conclusions are presented.

2 METHODOLOGY

In phase field approach a sharp crack Γ present in a body $\mathfrak{B}$ is regularized and represented as diffused crack Γ_l as shown in Figure 1. The body with a sharp crack, is subjected to traction and body forces, $\boldsymbol{f}_t$ and $\boldsymbol{f}_b$. The regularized crack function is written in terms of a scalar phase field order parameter representing the crack in the material as shown in Figure 2. The regularization of crack is given by,

$$\Gamma_l = \int_{\mathfrak{B}} \gamma(\vartheta, \nabla\vartheta) d\mathfrak{B} \tag{1}$$

The crack density function is defined as,

$$\gamma(\vartheta, \nabla\vartheta) = \frac{1}{2l_\vartheta}(\vartheta^2 + l_\vartheta^2 |\nabla\vartheta|^2) \tag{2}$$

The scalar fracture parameter $\vartheta(\boldsymbol{x})$ is obtained by minimization of Γ_l as,

$$\vartheta(\boldsymbol{x}) = e^{-\frac{|\boldsymbol{x}|}{l_\vartheta}} \tag{3}$$

The width of the regularized crack is given by length scale parameter, l_ϑ. As, $l_\vartheta \to 0$, $\Gamma_l \to \Gamma_l$ and transition of the crack parameter is seen from 0 to 1. $\vartheta(\boldsymbol{x})$ = 1 denotes a completely fractured state and $\vartheta(\boldsymbol{x})$ = 0 shows the uncracked condition of the material.

Anisotropic crack density function can be used to capture the material's directionality.

$$\gamma(\vartheta, \nabla\vartheta) = \frac{1}{2l_\vartheta}(\vartheta^2 + l_\vartheta^2 \nabla\vartheta \cdot \boldsymbol{A} \nabla\vartheta) \tag{4}$$

The structural tensor $\boldsymbol{A}$ denotes the direction of material along the fibers or the rolling direction with ω as a penalty parameter and $\boldsymbol{N}$ a directional tensor.

$$\boldsymbol{A} = \boldsymbol{I} + \omega\, \boldsymbol{N} \otimes \boldsymbol{N}, \qquad \boldsymbol{N} = \begin{bmatrix} cos\theta & sin\theta & 0 \end{bmatrix}^T \tag{5}$$

The total potential energy of the system is given by.

$$\Pi = \int_{\mathfrak{B}} \Psi(\boldsymbol{\varepsilon})\, \mathrm{d}\mathfrak{B} + \int_{\mathfrak{B}} G_c\, \gamma(\vartheta, \nabla\vartheta)\, \mathrm{d}\mathfrak{B} - \int_{\mathfrak{B}} \boldsymbol{f}_b \cdot \boldsymbol{u}\, \mathrm{d}\mathfrak{B} - \int_{\partial\mathfrak{B}} \boldsymbol{f}_t \cdot \boldsymbol{u}\, \mathrm{d}A \tag{6}$$

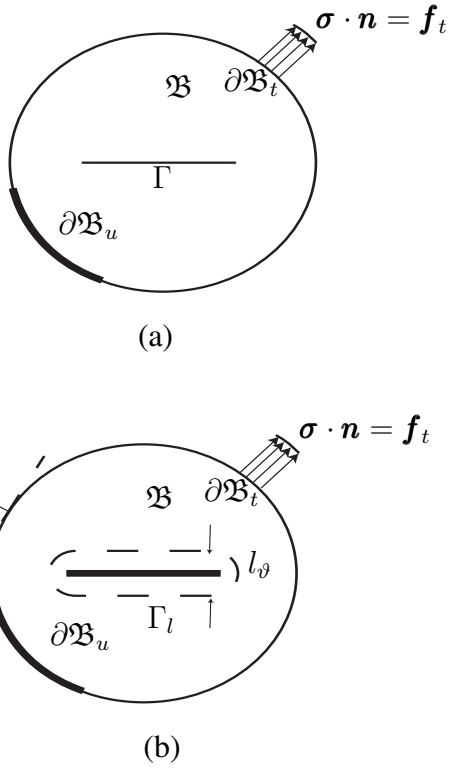

Figure 1: Representation of domain with (a) sharp crack (b) regularized crack

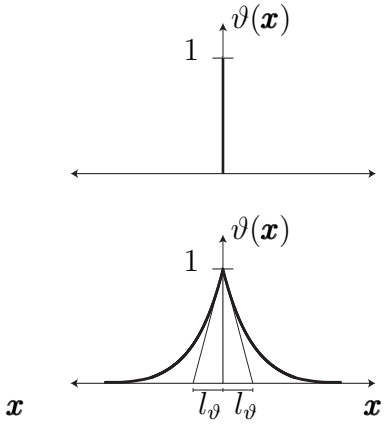

Figure 2: Sharp and diffused crack at $\boldsymbol{x}$ = 0

The elastic strain energy is split into volumetric and deviatoric parts.

$$\Psi^+ = \Psi^+_{vol} + \Psi_{dev} \quad and \quad \Psi^- = \Psi^-_{vol} \tag{7}$$

$$\Psi^{+} = \frac{1}{2}K_v < tr(\boldsymbol{\varepsilon}) >_{+}^{2} + \mu \boldsymbol{\varepsilon}_{dev} : \boldsymbol{\varepsilon}_{dev} \quad (8)$$

$$\Psi_{vol}^{-} = \frac{1}{2}K_v < tr(\boldsymbol{\varepsilon}) >_{-}^{2} \quad (9)$$

$$\boldsymbol{\varepsilon}_{dev} = \boldsymbol{\varepsilon} - \frac{tr(\boldsymbol{\varepsilon})}{3} \quad (10)$$

K_v is the bulk modulus and μ is the shear modulus of the material. For $< x >_{\pm} = \frac{x \pm |x|}{2}$

$$H_I = \max_{t\epsilon[0,T]} \Psi_{vol}^{+} \qquad H_{II} = \max_{t\epsilon[0,T]} \Psi_{dev} \quad (11)$$

H_I is the history parameter for elastic energy induced by volumetric dilation, and H_{II} is the history parameter for elastic energy induced by deviatoric deformation. G_{Ic} and G_{IIc} are critical fracture toughness values corresponding to modes I and II.

The structural equilibrium condition is obtained by the minimization of the total energy with respect to the deformation. Additionally, an evolution equation is defined by minimization of the free energy function. A finite element scheme is then adopted to solve these two equations. The evolution of fracture together with equilibrium is solved in a staggered approach. The equilibrium equation and evolution equation of damage are given by,

$$\nabla \cdot \boldsymbol{\sigma} + \boldsymbol{f}_b = \mathbf{0} \quad (12)$$

$$-2\left(1-\vartheta\right)\left(\frac{H_I l_\vartheta}{G_{Ic}} + \frac{H_{II} l_\vartheta}{G_{IIc}}\right) + \left(\frac{\vartheta}{l_\vartheta} - l_\vartheta \nabla^2 \vartheta\right) = 0 \quad (13)$$

3 NUMERICAL EXAMPLES

In this section, we present the numerical examples that are used to demonstrate the efficiency of the proposed model. A MATLAB code has been implemented in finite element frame work for the analysis. Three noded triangular elements are used for the analysis. Three examples are considered for analysis namely a) Rectangular plate with one inclined crack under mixed mode condition b) Rectangular plate with multiple inclined crack c) Wood specimen under mixed mode loading condtion. The numerical results are verified and validated by comparing with the results availabe in the litreature.

3.0.1 Rectangular plate with one inclined crack

A rectangular plate with an inclined crack example is considered for analysis under the mixed mode conditions. The rectangular plate is of dimensions 152.4x76.2 mm, as shown in Figure 3. A plane strain condition is considered for the analysis. The material properties for a rock-like material namely: Elastic modulus, E = 4.2 kN/mm^2, Bulk modulus, K_v = 3.5 kN/mm^2, critical fracture toughness for mode I, G_{Ic} = 5.0x10^{-6}kN/mm and mode II, G_{IIc} = 13G_{Ic} are considered for the analysis. These values are taken from the litreature [22]. The Poisson's ratio of the material is taken as 0.3. The plate is considered to be fixed at the bottom edge, and a displacement of 5x10^{-5}mm is applied on the top edge. The initial length of the central crack inclined at an angle of 30° is taken as 12.7 mm. Upon application of the compressive loading, there is an increase in crack length. Initially, the wing cracks are formed, followed by the formation of the secondary cracks as shown in Figure 4. The primary wing crack formation is attributed to the volumetric term present in the energy, and the deviatoric strain energy term helps in predicting the secondary crack formation. The wing crack formation and subsequent secondary crack growth are attributed to the pure tensile and shear modes associated with fracture. This is also clearly evident from the experimental results obtained from literature [25] of the same material as shown in Figure 5. This validates the fact that the present model is able to predict the mixed-mode anisotropic fracture.

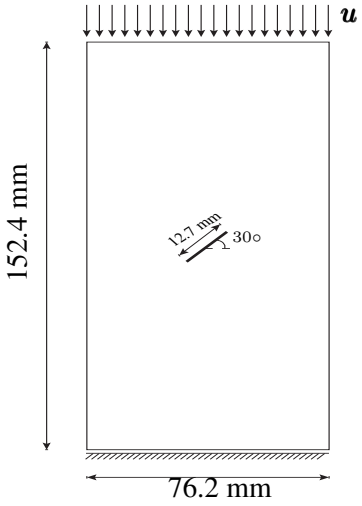

Figure 3: Geometry for rock with single fissure

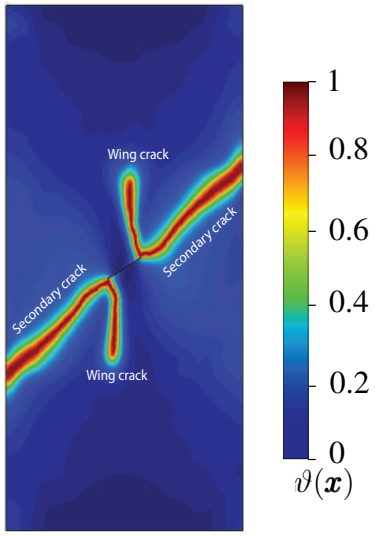

Figure 4: Evolution of phase field $\vartheta\,(\boldsymbol{x})$ for rock with single fissure

Figure 5: Experimental result of fracture in rock [25]

3.0.2 Rectangular plate with multiple inclined cracks

A rectangular plate with multiple inclined cracks example is considered for analysis under the mixed mode conditions. The rectangular plate is of dimensions 152.4x76.2 mm, as shown in Figure 6. A plane strain condition is considered for the analysis. The material properties for a rock-like material namely: Elastic modulus, E = 4.2 kN/mm^2, Bulk modulus, K_v = 3.5 kN/mm^2, critical fracture toughness for mode I, G_{Ic} = 5.0x10^{-6}kN/mm and mode II, G_{IIc} = 13G_{Ic} [22] are considered for the analysis. The Poisson's ratio of the material is taken as 0.3. The plate is considered to be fixed at the bottom edge, and a displacement of 5x10^{-5}mm is applied on the top edge. The initial length of the inclined cracks at an angle of 30° is taken as 12.7 mm. Two cases are considered here for analysis. In the first case, termed case A, two fissures are separated by a distance of 20 mm. This separation between the cracks is known as ligament length. In the second case, termed case B, three cracks are considered as depicted in figure 6. The third crack is between the two cracks with a bridging angle 60°.

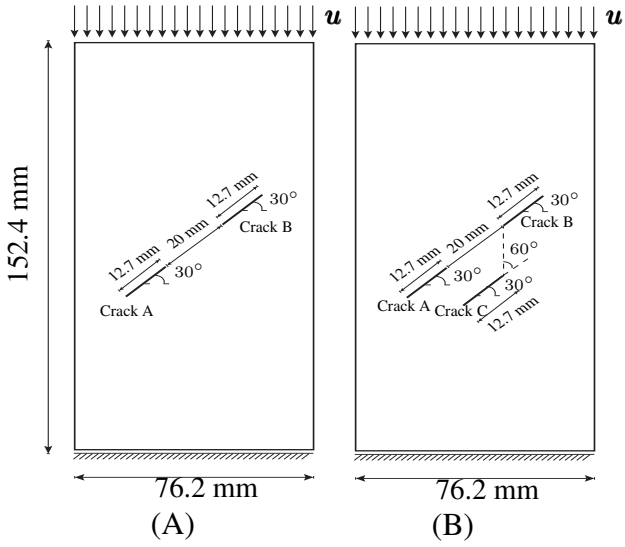

Figure 6: Geometry for rock with (A) 2 fissures (B) 3 fissures

The fracture in case A includes a shear crack due to compressive fields and a wing and secondary shear crack, as shown in Figure 7. The appearance of wing cracks is due to the pure tensile, and secondary cracks are because of the shear behavior of loading. The crack in ligament length is the coalescence of secondary shear and out-of-plane shear cracks. In the case of B, the presence of a third crack with a smaller ligament length results in the coalescence of cracks. The wing cracks of the third crack merge with those of the above two cracks. It is seen that the smaller ligament length and bridging angle result in the coalescence of cracks to a greater extent. Figure 8 shows the load-displacement response for all the above cases. The primary or wing cracks generally grow in the direction of the bedding plane of the rock [12]. At the same time, the orientation of secondary or shear cracks is not seen to grow along the direction of the bedding plane.

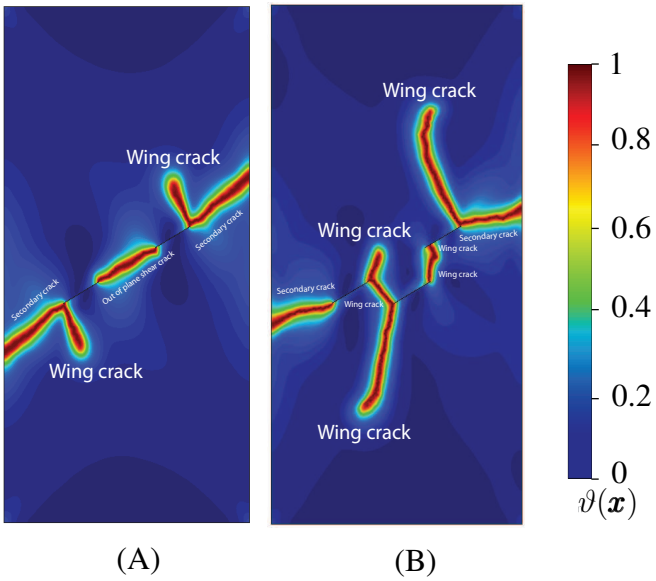

Figure 7: Evolution of phase field $\vartheta(\boldsymbol{x})$ for rock with (A) 2 fissures (B) 3 fissures

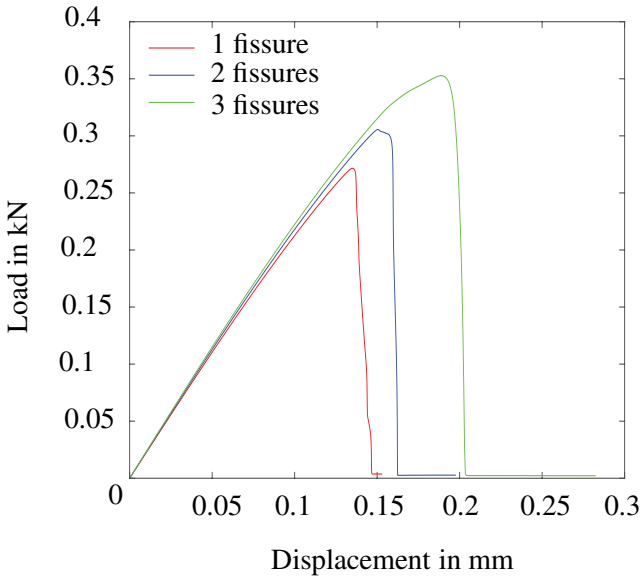

Figure 8: Load displacement response for rock

3.0.3 Mixed-mode fracture in wood

A circular arcan specimen of Russian pine wood with a 100 mm diameter is considered for the analysis. The crack length is 30 mm. The thickness of the specimen is considered as 0.3 mm. A plane strain condition is assumed for the analysis. The material properties of the wood are taken as elastic modulus, E_{11} = 4717.07 MPa, E_{22} = 163.539 MPa, and Poisson's ratio, ν_{12} = 0.344. The Shear modulus is considered as G_{12} = 226.420 MPa [26].

Table 1: Fracture toughness

Angle	G_{Ic} (N/mm)	G_{IIc} (N/mm)
10°	0.3065	0.3491
30°	0.24865	0.4554
40°	0.2108	0.6880

Wood, an orthotropic material, has its fiber orientation in a particular direction. The crack propagation in wood is mainly along the fiber orientation. This example aims to understand the behavior of anisotropy under mixed-mode conditions. The mode mixity ratio is changed by varying the inclination of the crack. The specimen is subjected to a tensile loading. An

inclined crack is considered along the fiber direction.

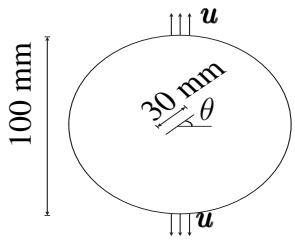

Figure 9: Geometry and boundary conditions for mixed mode fracture in wood

It is seen that the crack propagation in wood follows the path of fiber direction irrespective of crack angle. Figures 9 and 10 show the arcan specimen's geometric conditions and crack evolution as per the phase field model. Figure 11 shows the experimental results of the arcan specimen of wood. Phase field results are compared with the experimental results [26]. Figure 12 shows the load-displacement response for the wood specimen. In this case of the chosen parameters, the mode mixity is found to have very lttle influence on anisotropic fracture.

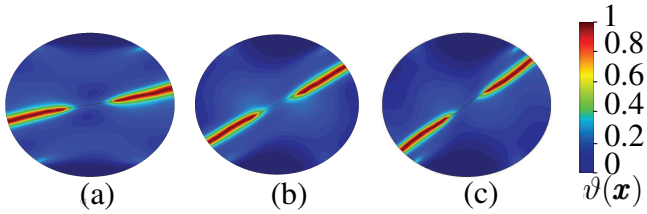

Figure 10: Evolution of crack phase field $\vartheta(\boldsymbol{x})$ for different angle of inclinations (a) 10° (b) 30° (c) 40°

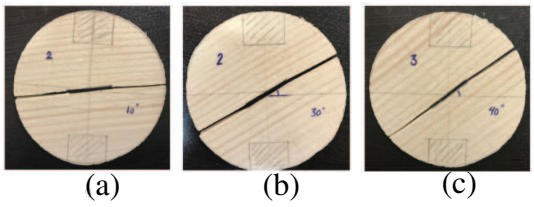

Figure 11: Experimental results [26] for mixed mode fracture in wood for different angle of inclinations (a) 10^o (b) 30^o (c) 40^o

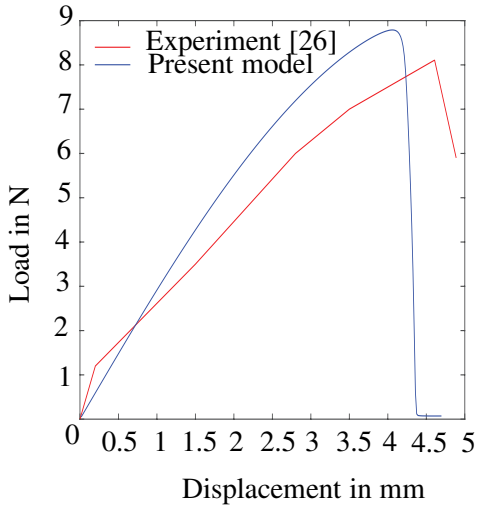

Figure 12: Load displacement response for wood

4 CONCLUSIONS

In this work, an anisotropic phase field model that accounts for mixed-mode fracture criteria has been formulated and implemented. It has been demonstrated through several examples that the mixed-mode criterion successfully captures the dominating fracture mode. This is evident from the presence of primary and secondary cracks in certain materials. The model is also able to predict mixed-mode fracture in wood-like materials.

REFERENCES

[1] Z. H. Stachurski, G. Wang, X. Tan. 2021. Chapter 6 - Magnetic properties of amorphous metallic alloys. *An Introduction to Metallic Glasses and Amorphous Metals*; pp. 157-192.

[2] H. Kirchmayr. 2001. Magnetic Anisotropy. *Encyclopedia of Materials: Science and Technology*; pp. 4754-4757.

[3] Takei A, Roman B, Bico J, Hamm E, Melo F (2013) Forbidden directions for the fracture of thin anisotropic sheets: an analogy with the Wulff plot. *Phys Rev Lett*, 110:144301.

[4] Pranavi, D., A. Rajagopal, and J. N. Reddy. 2021. Interaction of anisotropic crack phase field with interface cohesive zone model for fiber reinforced composites. *Composite Structures*, 270:114038.

[5] P. Zhang and X. Hu and TQ Bui and W. Yao. 2019. Phase field modeling of fracture in fiber reinforced composite laminate. *International Journal of Mechanical Sciences*, 161-162:105008.

[6] Li B, Maurini C (2019) Crack kinking in a variational phase-field model of brittle fracture with strongly anisotropic surface energy. *J Mech Phys Solids*, 125:502–522.

[7] Teichtmeister S, Kienle D, Aldakheel F, Keip M-A (2017) Phase field modeling of fracture in anisotropic brittle solids. *Int J Non-Linear Mech*, 97:1–21.

[8] Min, L., Hu, X., Yao, W., Bui, T. Q., Zhang, P. 2022. On realizing specific failure initiation criteria in the phase field model. *Computer Methods in Applied Mechanics and Engineering* 394:114881.

[9] Pranavi, D., and Rajagopal, A. 2021. Modeling anisotropic fracture in a metal-fiber reinforced composite system. *IOP Conference Series: Materials Science and Engineering*, 1166:012023.

[10] M. Kalina, V. Schöne, B. Spak, F. Paysan, E. Breitbarth, M. Kästner. 2023. Fatigue crack growth in anisotropic aluminium sheets — phase-field modelling and experimental validation. *International Journal of Fatigue*, 176:107874.

[11] Y. Tan and Y. He and X. Li. 2022. Phase field fracture modeling of transversely isotropic piezoelectric material with anisotropic fracture toughness *International Journal of Solids and Structures*, 248:111615.

[12] Y. Gao and Z. Liu and Q. Zeng and T. Wang and Z. Zhuang and K.-C. Hwang. 2017. Theoretical and numerical prediction of crack path in the material with anisotropic fracture toughness *Engineering Fracture Mechanics*, 180:330-347.

[13] S. Rezaei and J. Rezaei Mianroodi and T. Brepols and S. Reese. 2021. Direction-dependent fracture in solids: Atomistically calibrated phase-field and cohesive zone model *Journal of the Mechanics and Physics of Solids*, 147:104253.

[14] S. Zhang and D.-U. Kim and W. Jiang and M. R Tonk. 2021. A phase field model of crack propagation in anisotropic brittle materials with preferred fracture planes *Computational Materials Science*, 193:110400.

[15] Ambati, M. and Gerasimov, T. and D. Lorenzis, L. 2015. A review on phase-field models of brittle fracture and a new fast hybrid formulation. *Computational Mechanics*, 55:383-405.

[16] Kuhn, C. and Noll, T. and Müller, R. 2016. On phase field modeling of ductile fracture.*GAMM-Mitteilungen*, 39:35-54.

[17] Hofacker, M. and Miehe, C. 2013. A phase field model of dynamic fracture: Robust field updates for the analysis of complex crack patterns. *International Journal for Numerical Methods in Engineering*, 93:276-301.

[18] H. Amor and J.-J. Marigo and C. Maurini. 2009. Regularized formulation of the variational brittle fracture with unilateral contact: Numerical experiments. *Journal of the Mechanics and Physics of Solids*, 57:8.

[19] Miehe, C. and Welschinger, F. and Hofacker, M. 2010. Thermodynamically consistent phase-field models of fracture: Variational principles and multi-field FE implementations. *International Journal for Numerical Methods in Engineering*, 83:1273-1311.

[20] M.L. Benzeggagh and M. Kenane. 1996. Measurement of mixed-mode delamination fracture toughness of unidirectional glass/epoxy composites with mixed-mode bending apparatus. *Composites Science and Technology*, 56:439-449.

[21] Reeder, JR. 1992. An evaluation of mixed-mode delamination failure criteria.

[22] S. Liu and Y. Wang and C. Peng and W. Wu. 2022. A thermodynamically consistent phase field model for mixed-mode fracture in rock-like materials. *Computer Methods in Applied Mechanics and Engineering*, 392:114642.

[23] X. Zhang and Scott W. S. and C. Vignes and D. Sheng. 2017. A modification of the phase-field model for mixed mode crack propagation in rock-like materials. *Computer Methods in Applied Mechanics and Engineering*, 322:123-136.

[24] H. Yu and L. Hao and R. Shen and L. Guo and Z. Shen and Y. Li. 2022. A phase field model with the mixed-mode driving force of power-law relation. *Engineering Fracture Mechanics*, 264:108265.

[25] E.Z. Lajtai. 1971. A theoretical and experimental evaluation of the Griffith theory of brittle fracture. *Tectonophysics*, 11:129-156.

[26] Fakoor, M. and Manafi F., H. 2019. Mixed-mode I/II fracture criterion for crack initiation assessment of composite materials. *Acta Mech.*, 230:281-301.